energies

MDPI

Article

A Modeling Framework to Develop Materials with Improved Noise and Vibration Performance for Electric Vehicles

Seyed Jamaleddin Mostafavi Yazdi [1], Seongchan Pack [2], Foroogh Rouhollahi [3] and Javad Baqersad [1,*]

[1] Department of Mechanical Engineering, Kettering University, 1700 University Ave, Flint, MI 48504, USA
[2] Global Product Development at Global Technical Center, General Motors, Warren, MI 48340, USA
[3] Department of Chemical Engineering, Kettering University, 1700 University Ave, Flint, MI 48504, USA
* Correspondence: jbaqersad@kettering.edu

Abstract: The automotive and aerospace industries increasingly use lightweight materials to improve performance while reducing fuel consumption. Lightweight materials are frequently used in electric vehicles (EVs). However, using these materials can increase airborne and structure-borne noise. Furthermore, EV noise occurs at high frequencies, and conventional materials have small damping. Thus, there is an increasing need for procedures that help design new materials and coatings to reduce the transferred and radiated noise at desired frequencies. This study pioneered new techniques for microstructure modeling of coated and uncoated materials with improved noise, vibration, and harshness (NVH) performance. This work uses the microstructure of materials to study their vibration-damping capacity. Images from an environmental scanning electron microscope (ESEM) show the microstructure of a sample polymer and its coating. Tensile tests and experimental modal analysis were used to obtain the material properties of the polymer for microstructure modeling. The current work investigates how different microstructure parameters, such as fiberglass volume fraction and orientation, can change the vibration performance of materials. The damping ratio in the study was found to be affected by changes in both the direction and volume ratio of fiberglass. Furthermore, the effects of the coating are investigated in this work. Through modal analysis, it was observed that increasing the thickness of aluminum and aluminum bronze coatings caused a rightward shift in resonance frequency. Coatings with a thickness of 2 mm were found to perform better than those with lower thicknesses. Furthermore, the aluminum coating resulted in a greater shift in frequency than the aluminum bronze coating. Additionally, the coating with a higher damping ratio (i.e., aluminum bronze) significantly reduced the amplitude of surface velocity due to excitation, particularly at higher frequencies. This study provides engineers with an understanding of the effects of layer coating on the NVH performance of components and a modeling approach that can be used to design vehicles with enhanced noise and vibration performance.

Keywords: vibration; damping; NVH; lightweight; electric vehicles; finite element analysis

Citation: Mostafavi Yazdi, S.J.; Pack, S.; Rouhollahi, F.; Baqersad, J. A Modeling Framework to Develop Materials with Improved Noise and Vibration Performance for Electric Vehicles. *Energies* **2023**, *16*, 3880. https://doi.org/10.3390/en16093880

Academic Editor: Oscar Barambones

Received: 16 March 2023
Revised: 27 April 2023
Accepted: 28 April 2023
Published: 3 May 2023

1. Introduction

Recently, lightweight materials such as aluminum, plastic, carbon fiber, and composites have been increasingly used in the automotive body structure and aerospace industries to reduce fuel consumption while maintaining or improving safety and performance. The recent advances in battery technology, novel materials, and infrastructure are key trends that can significantly increase the adoption of battery electric vehicles (BEVs). Lightweighting can help reduce the cost of electric vehicles (EVs) and result in a significant cost reduction for the consumer [1]. Additionally, lightweight EVs require less energy to accelerate and maintain speed, which can help to alleviate range anxiety [2]. Automotive engineers have the challenge of reducing vehicle weight to meet new vehicle emission standards [3,4]. Lighter vehicles with better performance and fuel efficiencies are especially vulnerable to higher in-cabin structure and airborne noise levels. Because the body panels radiate most

structural vibrations in cars [5], particular care must be paid to modeling these lightweight structures. Furthermore, the recent increase in EVs production has highlighted the need to minimize noise generated by the propulsion system in these vehicles [4]. EVs are quiet; thus, with the lack of an engine to mask noise from other components, the sound from the electric motor and other noise sources becomes more prominent [6]. The prolonged high-frequency sounds from electric motors and other EV components can be unpleasant for passengers. Thus, there is an increasing need for designing materials and coatings that can reduce the transferred and radiated noise. Recent developments in electric vehicles have highlighted the need for materials with improved noise, vibration, and harshness (NVH) and high electromagnetic shielding interference (EMI) [7].

Structural vibration can cause structure-born noise and is very critical for noise reduction. Recently, researchers have tried to focus on providing structural vibration for electric vehicles [4,8–10]. Yang et al. [11] reviewed the vibration of structures using different tuned mass damper models. Materials with improved noise and vibration performance are a significant area of interest in NVH [12–14]. The dynamic behavior of different NVH applications was modeled using nonlinear dynamical systems (SINDy) [15]. Researchers have investigated different materials to reduce interior noise in cars. Aluminum became the preferred material for sound silencer coatings due to its low weight, which is three times less than steel [16]. To minimize the interior and exterior noise of the engine, asbestos and slag wool were effective in absorbing the noise because they are porous materials [17]. The vibration of functionally graded porous structures was investigated to study the effect of porosity distribution patterns on their vibrational properties [18–21]. Previous research has studied the free vibration of sandwich panels with functionally graded material (FGM) [22]. A new approach was proposed that reduces the order of the governing differential equations of Euler–Bernoulli for the buckling and vibration analysis of FGM and it achieved high accuracy [23]. Liao et al. [24] used composite materials, including polyester-polypropylene and butyl rubber, to decrease the noise in the hybrid electric vehicle. The damage detection and structural health monitoring of composite materials were performed using digital image correlation (DIC) and acoustic emission (AE) [25].

Some researchers have used experimental techniques for the microstructure characterization of materials [26–28]. Structural vibrations are usually measured using accelerometers, but recently non-contact techniques have received more attention [29–32]. Burdess et al. [33] used a laser Doppler vibrometer to develop an algorithm for characterizing the microstructure properties of materials. Xiong et al. [34] proposed a non-contact laser excitation for the modal analysis of microstructures. In that work, the dynamic response of micro-electro-mechanical systems (MEMS) was used for extracting the modal parameters of microstructures. In a publication by Zhou et al. [35], an acoustic-excitation optical coherence vibrometer (AE-OCV) was developed to measure the vibration of microstructures [35]. These experimental studies need to be integrated with numerical modeling approaches to develop a framework for developing new materials with superior vibration properties.

Microstructure modeling has been extensively used in material science for designing materials with superior static and fatigue behavior [36–40]. Herriott et al. [41] developed a multi-scale framework for predicting material properties in additive-manufactured materials. Microstructure modeling has also been used for creep prediction in composites [42]. The microstructure of materials can affect their vibrational properties [43]. Hence, there has been an increasing interest in the microstructures of materials in recent years and their effect on their mechanical properties. Amirian et al. [44] studied the effect of microstructure changes in metals on vibrational properties using modal tests and finite element analyses. They found that the changing microstructures could significantly affect the damping loss factor. Damir et al. [45] used modal analysis to characterize the fatigue behavior in austempered ductile iron (ADI). They showed that the damping ratio changed with the iron hardness and fatigue life. Several approaches, such as representative volume element (RVE), were used to model the fibers in the microstructure. Our study is innovative and straightforward as it includes the fibers and their direction in the microstructure. This approach

provides more flexibility and allows the exploration of the structure's microstructural research for any mechanical analysis, such as dynamic and vibration analysis. Additionally, another innovation of our study is to consider the microstructure for the NVH analysis of full-size structures. Despite the extensive work on using microstructure modeling for static studies, the number of studies that evaluate microstructure modeling to study the vibration properties of structures is limited. Most researchers only consider macro-level modeling [46–49] in vibration analysis.

The current work proposes a novel experimental and numerical scheme to optimize the NVH behavior of coated automotive components. This work tries to use DREAM.3D models, which are conventionally used for quasi-static analysis, for dynamic and noise analysis. The proposed approach of using DREAM.3D models to perform dynamic analysis, obtain vibration and acoustic response, and investigate the effects of damping is innovative and has not been explored before. The project results can be used to design and optimize the vibration performance of materials. The work integrates state-of-the-art testing and simulation techniques to analyze the performance of coated components. This study's proposed methodology and results can help engineers design vehicle structures with improved NVH performance.

The present work studies the microstructure model of PEEK with different volume fractions and fiber orientations. Section 2 discussed the materials and methods that were used in the paper. The section describes how the models were created in Dream3D and how material properties for each component were obtained. Section 3 shows the results of the analysis. This section shows the SEM images of the materials and the results of the finite element analysis of the models. The section also shows how the vibration response can be used to evaluate the acoustic performance of the materials. A finite element model of the PEEK microstructure is presented, and the effect of fiber volume fraction and direction on the NVH behavior is investigated. Then, the effect of adding aluminum and aluminum bronze coatings on the NVH behavior of actual structures with a base of PEEK material is studied.

2. Materials and Methods

This study proposes a methodology that can use finite element (FE) analysis and the microstructure of materials to optimize the performance of lightweight structures. Multi-scale modeling approaches have been utilized in this work. A schematic of the optimization process is shown in Figure 1. The volume ratio and the direction of fibers in the microstructure model are the optimization variables, and the effective damping ratio and the natural frequency are the goals of the optimization process. The fibers were distributed randomly in the polymer with different volume ratios from 0% to 50%. As can be seen, the process starts with microstructure modeling. In the first step of the modeling, the microstructure parameters are adjusted to obtain and evaluate how different parameters, such as the volume fraction in microstructures, can change the material properties. As illustrated in Figure 1, two microstructure models are used to obtain the material properties for the coating and substrate separately. The microstructures can have different micro-textures. FE models of these microstructures are used to evaluate the static and dynamic performance of the micromodel. A static model obtains density (ρ) and elasticity (E). A dynamic simulation (i.e., complex eigensolution or direct steady-state analysis) can obtain damping properties (e.g., ζ). The microstructure is excited, its response is measured, and the damping ratio is extracted from the fast Fourier transform (FFT). The parameters from the microstructure model are imparted to the macro model for vibration analysis. This process can be an optimization process to identify a structure with desired vibration properties. After extracting the mechanical properties of the microstructure from the tensile and dynamic simulations, the comparable properties were applied to the full-scale model. Then, a complex eigensolution was performed on the model using Abaqus, and modal properties such as resonance frequency and mode shapes were obtained for different fiberglass volume fractions and coatings.

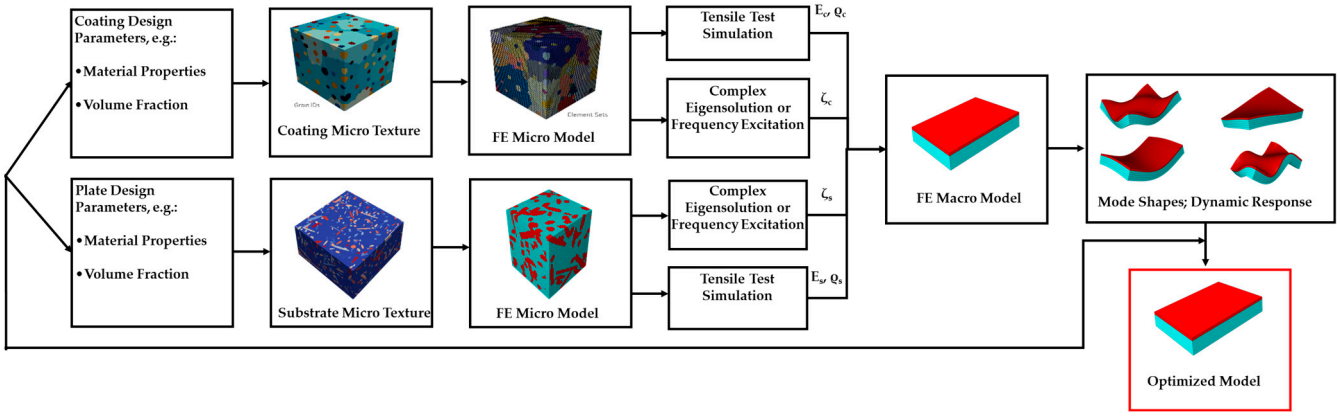

Figure 1. A schematic of the optimization process.

2.1. Microstructure Model

In the manufacturing process of fiber-reinforced polymers, the volume fraction and orientation can be used to adjust the material properties of the polymer. Several models of microstructures for PEEK were created using DREAM.3D [50], as shown in Figure 2. DREAM 3D generated fiberglass polymers with different volume fractions and orientations of fibers. In the first step, a microstructure model of the polymer was reinforced with 5 µm-diameter glass fiber. The fibers were distributed randomly in the polymer. By contrast, in the last two cases of Figure 2, the orientation of fibers was used horizontally and vertically to study how different directions can change the material properties and damping of the polymer.

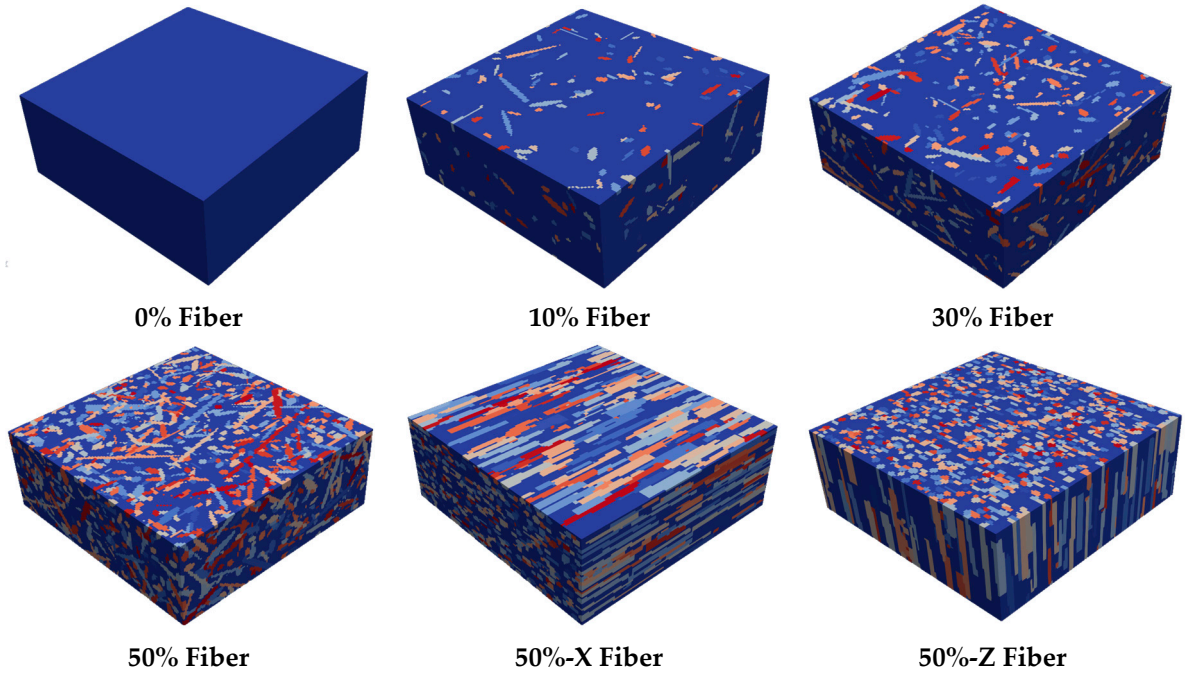

Figure 2. Different microstructure models created using DREAM 3D.

2.2. Elasticity and Hyperelastisity Obtained Using Tensile Test and EMA Data

An ASTM standard D638M-10 [51] tensile test was used to obtain the elastic properties of the polymer. As shown in Figure 3, the elasticity of the sample was calculated by finding the slope of stress–strain data in the linear region (i.e., 3833 Mpa). Because most vibrations occur in low amplitudes, the linear part of the curve can effectively model the elastic properties of the polymer.

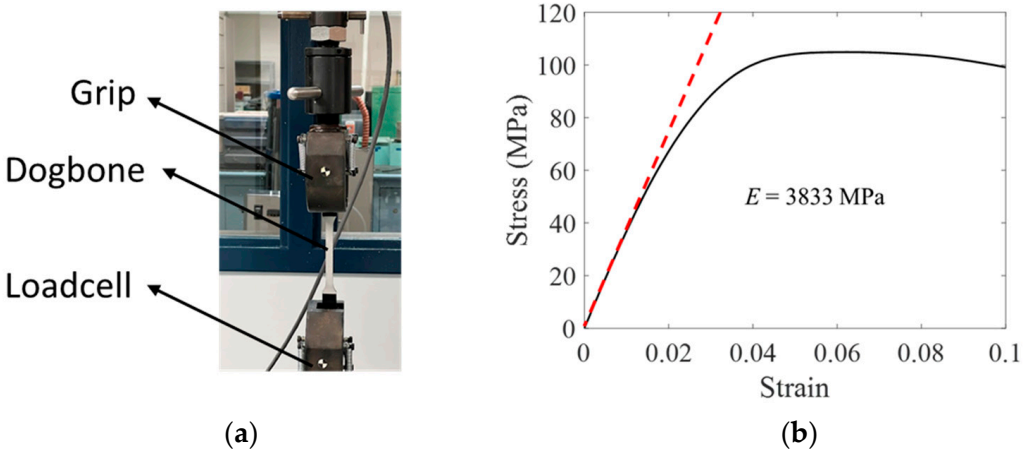

Figure 3. (**a**) The tensile test setup and (**b**) calculating the elasticity of samples from the stress–strain curve data.

2.3. Material Calibration for FEA Process

Polymers are frequently used in vehicles. In this study, PEEK, widely used in the auto industry [52], was selected to investigate the effect of microstructure and coating on vibrational properties. This section describes how elastic properties and damping for PEEK were obtained using tensile tests and experimental modal analysis (EMA). A flowchart of the material calibration is shown in Figure 4. The tensile tests were used to obtain the elastic properties. The EMA was used to validate the elastic properties and to estimate the damping values. The process is explained in detail below.

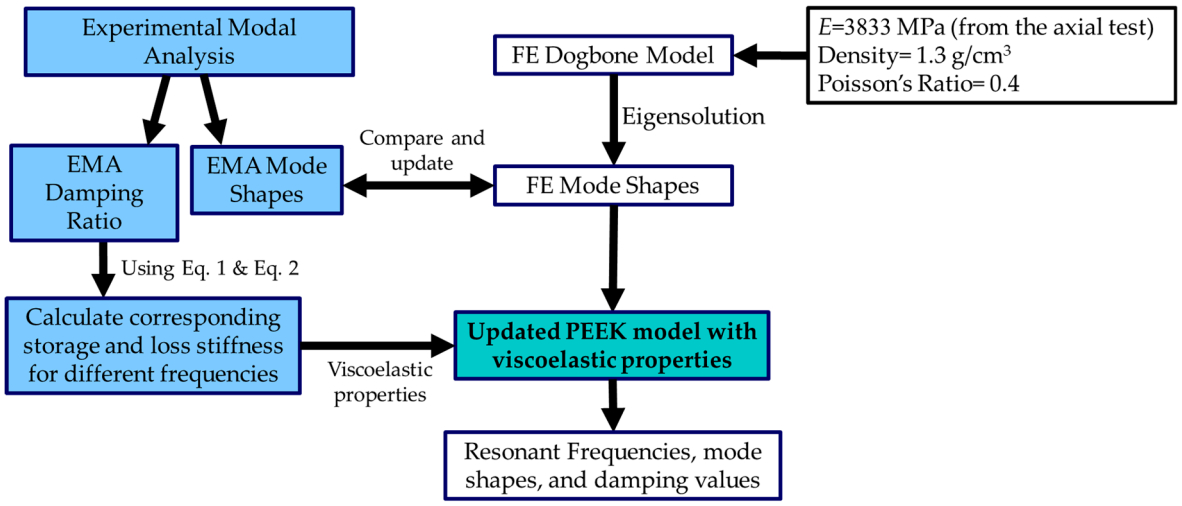

Figure 4. Flowchart showing how modal analysis and tensile tests were used to obtain and calibrate the elastic and damping properties of the polymer.

2.4. Validating FEA Model for PEEK Using Experimental Modal Analysis

An experimental modal analysis (EMA) was performed on the structure to validate the FE model. An impact hammer modal test was performed on dog bone specimens made of PEEK. The roving impact hammer method was implemented on all test samples with the accelerometer at a fixed location. To minimize mass-loading effects, a tear-drop accelerometer, which has a tiny mass, was used to capture the response. Two layers of bubble wrap were used as the base to replicate the free–free condition of the dog bone specimen, as shown in Figure 5. A total of 10 points were marked on the dog bones.

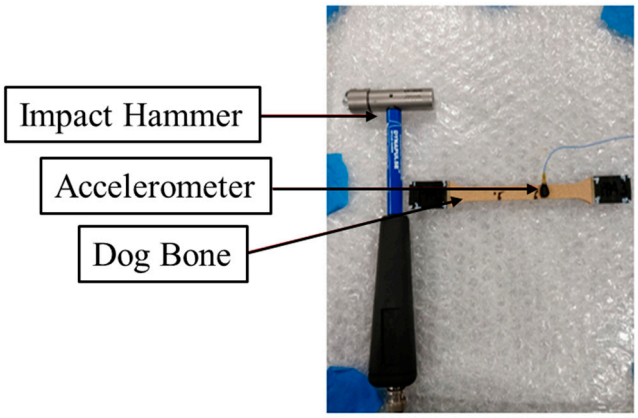

Figure 5. Dog bone in free-free condition.

2.5. Extracting the Viscoelastic Properties of Samples Using EMA

The EMA results provided damping values for each mode of the dog bone specimen. The damping ratio was obtained using the frequency response function (FRF) from the experimental modal analysis. A curve-fitting process was performed, and damping was calculated from the FRF for each resonant frequency. This damping value can be imparted in the FEA model to ensure the damping is appropriately considered.

In modal analysis, the damping is represented using EMA's damping ratio (ζ). The viscoelastic properties of PEEK were calculated using the elastic properties and damping ratio.

$$E' = E^{*}\cos(\zeta) \tag{1}$$

$$E'' = E^{*}\sin(\zeta) \tag{2}$$

Equations (1) and (2) represent the storage, E', and loss moduli, E'', respectively, and E^{*} is the elastic modulus. In this study, we assumed that the storage and loss moduli are constant at different frequencies for data simulation. Table 1 shows the calibrated material properties of the PEEK applied to the FEA model.

Table 1. Material properties of PEEK used for simulation.

E^{*} (MPa)	3832.3
ζ-Damping Ratio	0.0185
E'(MPa)	3831.61
E'' (MPa)	71.3
ν	0.4
$\rho\left(\mathrm{Kg/m^3}\right)$	1300

3. Results and Discussion

3.1. Scanning Electron Microscopy

A Philips FE1 Quanta 200 environmental scanning electron microscope (ESEM) was used to image polyetheretherketone's microstructure (PEEK) and PEEK with an aluminum coating. As shown in Figure 6a, the ESEM secondary micrograph of the PEEK sample shows dark reflective regions. The ESEM image shows a dense homogenous microstructure with no significant damage for PEEK with a relatively uniform surface. The homogenous microstructure of the PEEK allows us to create a homogenous finite element model. Additionally, Figure 6b illustrates the backscattered image of the PEEK with an aluminum coating. Figure 6a has a higher magnification (3660×) than Figure 6b (272×). Additionally, the aluminum coating covers the entire surface and has a less homogenous microstructure than the substrate. The manufacturing process was performed to have fewer defects, such as pores and gaps. The aluminum coating was deposited on the PEEK material to improve

the adhesion of the interface. All glass fiber-reinforced PPA, PPS, and PEEK were provided by Solvay Specialty Polymers. They were molded using an injection molding process. A thermal spray process applied zinc or aluminum or aluminum-bronze coatings. The size of the matrix in the microstructure was obtained using ESEM images.

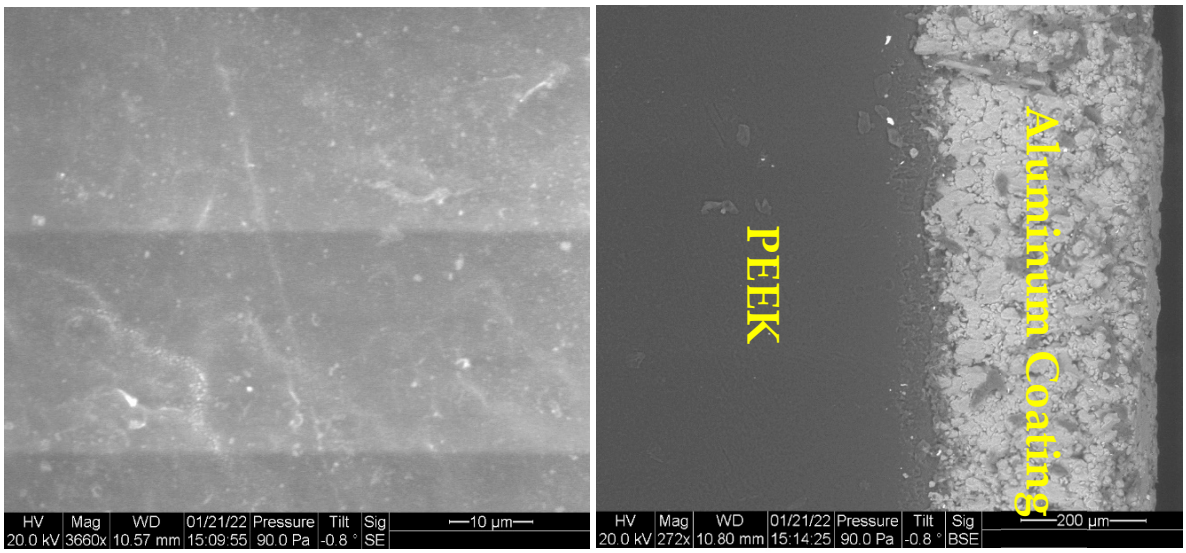

(**a**) (**b**)

Figure 6. ESEM images of (**a**) PEEK surface and (**b**) PEEK with aluminum coating.

3.2. EMA Analysis for PEEK Dogbone

The EMA's resonant frequencies and mode shapes validated the finite element model. The finite element model was created using solid elements in Abaqus. An eigensolution was performed on the model to obtain the model's resonant frequencies and mode shapes. The mode shapes can be extracted using the dog bone's reference degree of freedom (DOFs) modes. We show the reference points and the mode shapes in Figure 7. The figure shows a comparison between the FE and EMA mode shapes. As can be seen, there is a strong correlation between the EMA and FEA results. This can validate that the density and elasticity of the PEEK used in the FEA model represent the actual properties of the material.

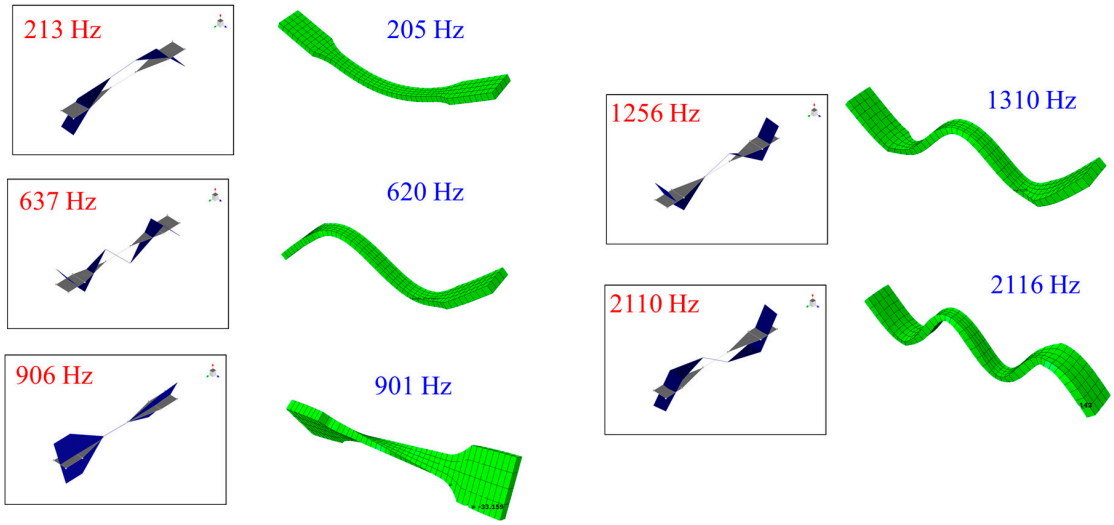

Figure 7. A comparison between resonant frequencies and mode shapes of the PEEK dog bone specimens using experimental modal analysis and the finite element method.

3.3. Finite Element Modeling of Microstructure

This section describes how a microstructure was developed and used to study the damping of the PEEK fiberglass composite.

3.3.1. FEA of the Microstructure Models

In this section, the FE model of the microstructures was created in Abaqus. Eight-node linear brick elements (C3D8) [53] with an element size of 1 µm were used for the models. This element size allows five elements along the diameter of the glass fibers. The material properties obtained for PEEK using EMA and tensile tests were applied to the model. For the fiberglass, nominal values were used. The finite element simulation can compare different models, as shown in Figure 8.

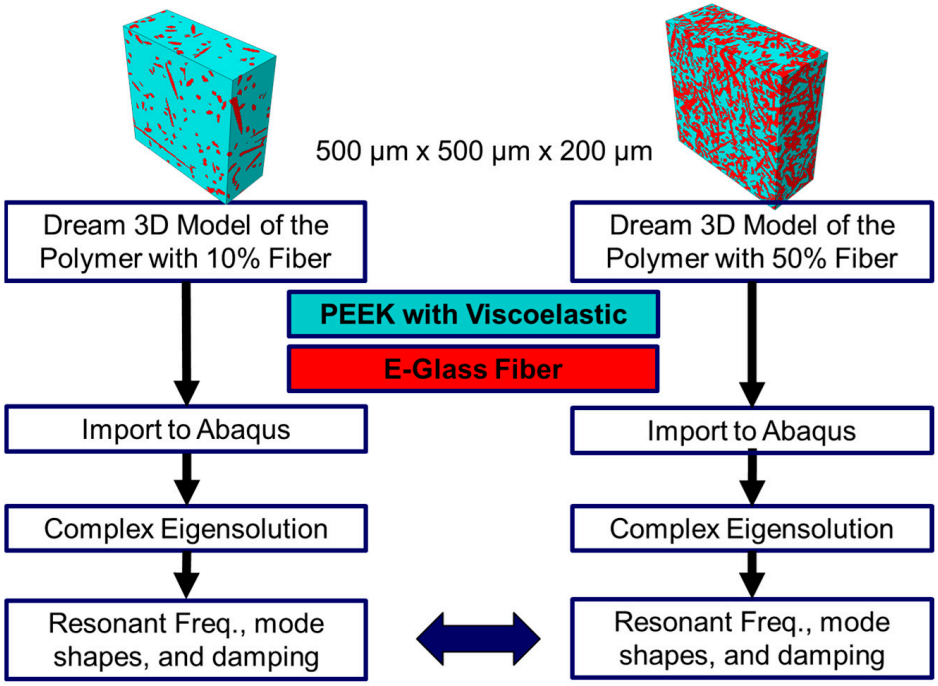

Figure 8. Flowchart of FEM of the microstructure using Abaqus.

The microstructure model was used to obtain the material properties of the composite for the actual structure. It should be noted that the macro model of an existing structure could not be directly developed using the microstructure with different volume fractions because it has high computational costs. Thus, the material properties for the macro model were obtained from the micromodel simulation. A complex eigensolution was performed on the model to obtain the microstructure's mode shapes and resonant frequencies. The complex eigensolution provides resonant frequencies, mode shapes, and damping values for the composite model (see Figure 9). The damping values were used in the macro model. These dynamic properties could also be obtained using direct frequency analysis. This type of analysis would allow for frequency-dependent material properties but would have higher computational costs.

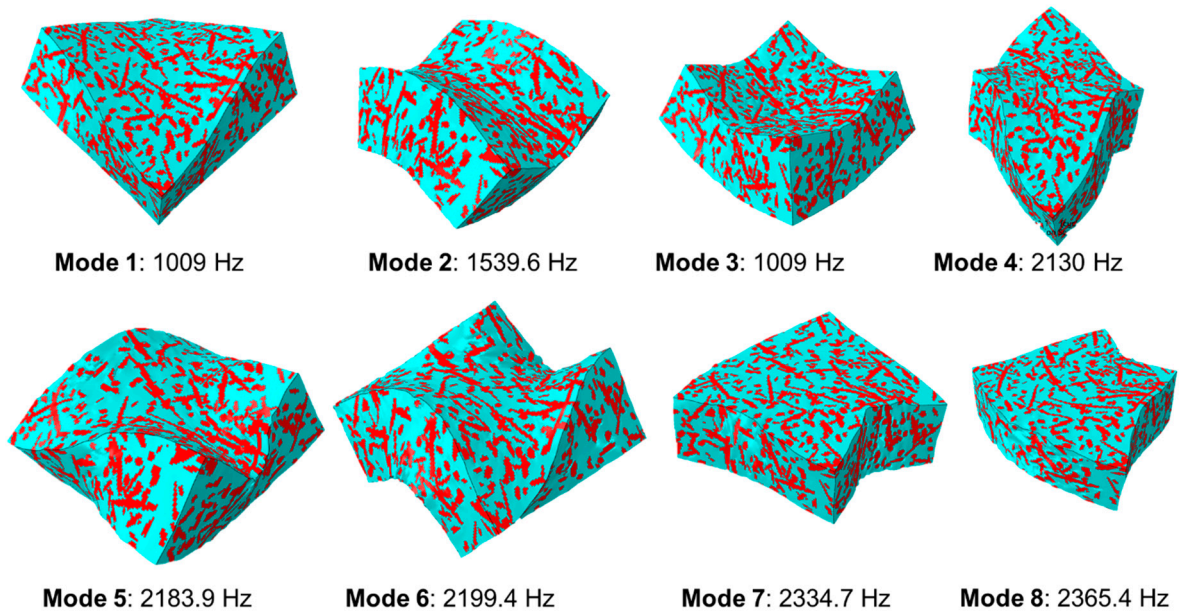

Figure 9. Eight mode shapes of the PEEK microstructure model with 30% fiberglass and their frequencies using Abaqus.

3.3.2. Effect of the Microstructure Fiberglass Volume and Orientation on NVH Performance of Materials

A list of resonant frequencies and damping values obtained using the microstructure model for the fiber-reinforced PEEK is shown in Table 2. As can be seen, increasing the fiber volume fractions in PEEK could decrease the damping ratio, while for a specific fiber volume ratio, for example, PEEK with 50% fiberglass, in different orientations (X and Z), the PEEK with 50% fiberglass volume ratio in the Z direction has the higher damping ratio. The damping ratio of PEEK with a 50% fiberglass volume fraction in a random direction has a lower value compared to fibers in the X and Z directions. We assumed in this study that friction between the fibers and the polymer is negligible. It can be observed that the damping ratio of PEEK is affected by the fiber volume of the PEEK and fiber direction. With increasing fiber volume fraction, the interaction among fibers also increases, and the damping ratio (friction) of PEEK is increased. The effects of contact and friction between the fibers and polymer can be studied to see how this contact can affect the noise behavior of the composite.

Table 2. The frequency and damping ratios of PEEK with fiberglass at different fiber volumes.

	0% Fiber		10% Fiber		20% Fiber		30% Fiber		50% Fiber		50 Fiber-X		50% Fiber-Z	
	Freq (Hz)	Damp. Ratio	Freq ((Hz)	Damp. Ratio	Freq ((Hz)	Damp. Ratio	Freq (Hz)	Damp. Ratio	Freq (Hz)	Damp. Ratio	Freq (Hz)	Damp. Ratio	Freq (Hz)	Damp. Ratio
1	569	0.36%	577	0.30%	585	0.27%	597	0.24%	613	0.19%	697	0.27%	620	0.29%
2	922	0.46%	958	0.50%	1007	0.48%	1071	0.43%	1168	0.31%	1422	0.39%	1188	0.46%
3	1318	0.98%	1442	0.65%	1532	0.46%	1613	0.35%	1706	0.23%	1975	0.29%	1733	0.34%
4	1810	1.38%	2059	0.98%	2258	0.70%	2438	0.52%	2651	0.32%	3121	0.33%	2818	0.39%
5	2097	1.29%	2412	0.94%	2675	0.67%	2918	0.49%	3201	0.29%	3814	0.34%	3273	0.43%
6	2570	0.60%	2721	0.57%	2893	0.51%	3101	0.45%	3413	0.31%	4164	0.39%	3470	0.47%
7	3355	1.04%	3766	0.88%	4162	0.69%	4570	0.53%	5090	0.33%	6183	0.37%	5230	0.48%
8	4328	1.69%	5203	1.24%	5900	0.57%	6380	0.48%	7082	0.33%	8670	0.40%	7202	0.48%
9	5050	0.83%	5477	0.68%	5972	0.89%	6708	0.64%	7546	0.32%	9154	0.38%	7765	0.46%
10	5277	0.96%	5805	0.76%	6300	0.61%	6829	0.49%	7636	0.38%	9197	0.37%	8013	0.48%
11	5569	1.83%	6847	1.41%	8056	0.53%	8618	0.46%	9432	0.32%	11,530	0.39%	9594	0.48%
12	7142	0.70%	7582	0.61%	8067	1.05%	9329	0.78%	10,572	0.31%	12,725	0.37%	10,907	0.44%
13	7257	1.20%	8166	0.85%	8906	0.62%	9631	0.48%	11,048	0.47%	13,887	0.44%	11,502	0.60%
14	7440	1.52%	8780	1.17%	9941	0.64%	10,848	0.52%	12,140	0.34%	14,926	0.40%	12,349	0.50%
15	8197	1.03%	9102	0.80%	10,034	0.91%	11,349	0.70%	13,196	0.44%	16,473	0.44%	13,879	0.55%

3.4. Investigating the Effects of Damping in a Sample Automotive Component

A model for a sample automotive component was developed to investigate how the micro-modeling of materials can be used to design automotive components with improved NVH behavior.

3.4.1. Using the Micro Model to Obtain Properties for Real Structure

The properties for the full-scale model were obtained from the micro model. The microstructures created in Section 2 were used for this study. A tensile test was performed on each microstructure to obtain the elastic properties of the compound. The microstructure model was clamped, and a tensile force was applied to the right face of the microstructure model using a multipoint constraint in Abaqus. The flowchart in Figure 10 illustrates extracting the elastic properties from the macro model. The damping properties for each case shown in Table 2 were used in the micro model.

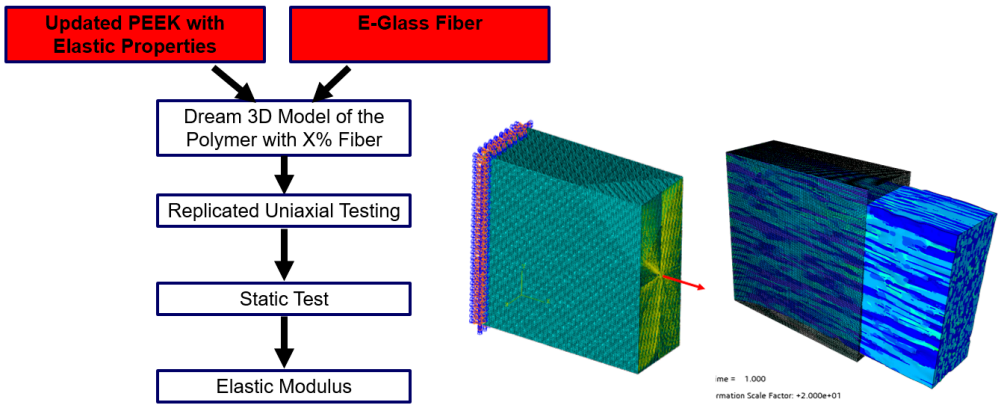

Figure 10. Flow chart of obtaining the properties of the macro model in Abaqus.

3.4.2. Coating and Damping in the Full-Scale Structure

After extracting the elastic modulus, density, damping, and Poisson's ratio of the microstructure from the tensile and dynamic simulations, the comparable properties were applied to the full-scale model (see Figure 10). Then, a complex eigensolution was performed on the model using Abaqus, and modal properties such as resonance frequency and mode shapes were obtained for different fiberglass volume fractions and coatings. Figure 11 shows the extraction and modeling of full-scale structures with fiberglass microstructures.

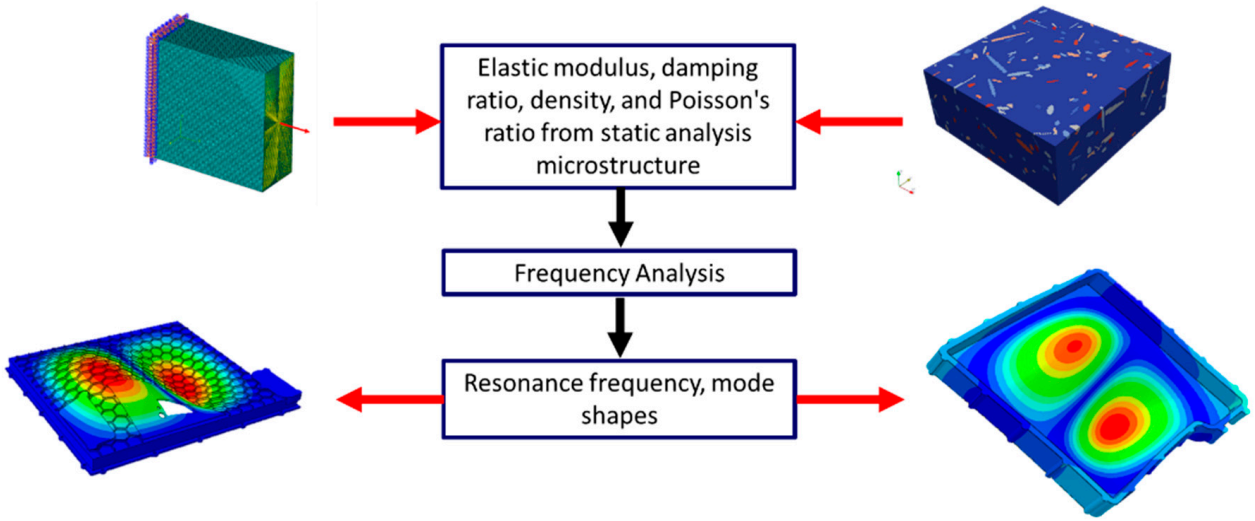

Figure 11. Modal analysis of the sample automotive structure using Abaqus.

3.4.3. Effects of Volume Fraction and Orientation of Fiberglass

Resonant frequencies and mode shapes of a full-scale structure with fiberglass microstructures were obtained using modal analysis in Abaqus (see Figure 12). Different fiberglass volumes fractions such as 0%, 10%, and 50% were considered for the microstructure of the model. It can be seen from Table 3 that the resonance frequency of the structure is increased with fiberglass volume fractions, and the model with 50% fiberglass in the X-direction has the highest resonance frequency. The frequency of 50% fiber volume in the X direction increased by 115% compared with 0% fiber. The frequency of 50% fiber volume in the X direction is greater than the 10% and 50% fibers.

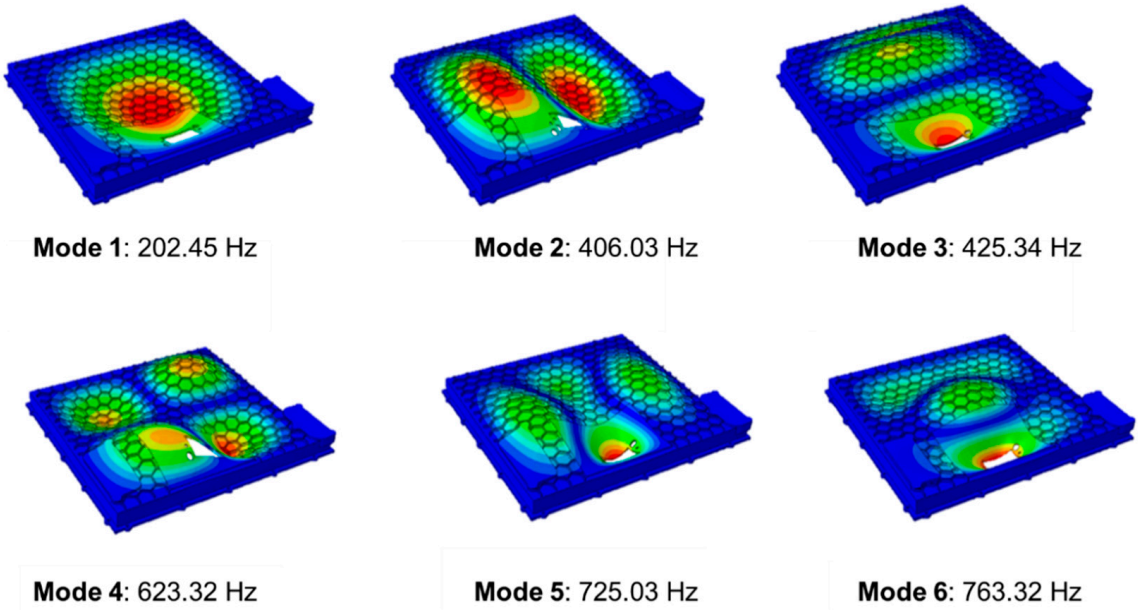

Figure 12. The first six mode shapes of the sample automotive component.

Table 3. Comparison of different modes of fiberglass.

	Frequency (Hz)			
Mode/Microstructure	**0% Fiber**	**10% Fiber**	**50% Fiber**	**50% Fiber (X-Direction)**
Mode 1	100.93	124.64	202.45	267.74
Mode 2	202.14	249.7	406.03	536.99
Mode 3	210.94	260.8	425.34	562.52
Mode 4	309.85	382.87	623.32	824.36
Mode 5	360.02	445.04	725.03	958.88
Mode 6	378.14	467.57	763.32	1009.5

3.4.4. Adding a Coating Layer

To avoid the airborne noise level and reduce the weight of the structure for fuel consumption, different coating materials are added to lightweight materials. In this section, we investigated the effects of different coatings on the vibrational properties of the full-scale model. When a coating is applied to a material, it can alter the way the material responds to external vibrations, such as those induced by an impact or a mechanical force. This is due to the changes in the stiffness, damping, and mass properties of the coated material, as well as the interface between the coating and the substrate. These changes can result in modifications to the natural frequencies and modes of vibration of the coated material. The coating can shift the frequency response of the structure and can impact the amplitude of the response. Different coatings made of aluminum and aluminum bronze were sprayed

on the model's base made of PEEK with 0% and 50% fiberglass volume fractions. Figure 13 shows aluminum and aluminum bronze coatings on the structure.

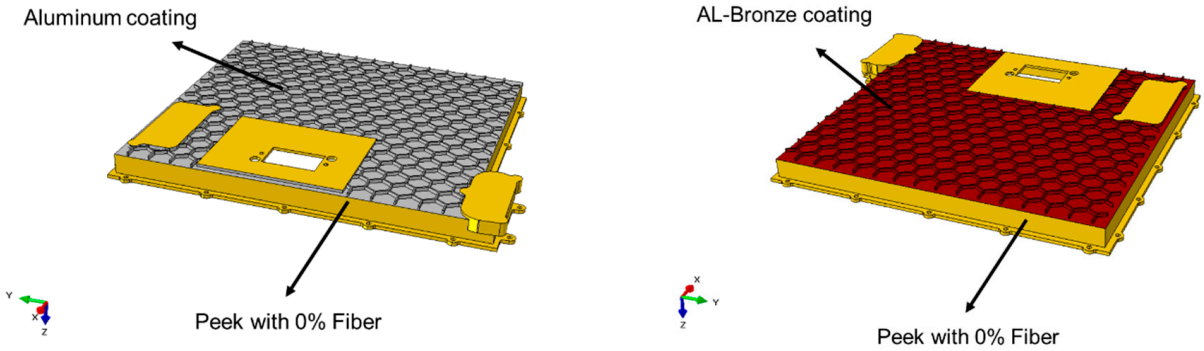

(**a**) Aluminum coating (**b**) Aluminum bronze coating

Figure 13. Different coatings on the structure: (**a**) aluminum (**b**) aluminum bronze.

To start the modal analysis using Abaqus, the material properties of aluminum and aluminum bronze were considered for the study (see Table 4). The material properties provided by the manufacturer were used in this analysis.

Table 4. The material properties of aluminum and aluminum bronze.

Material	Density (g/cm^3)	Young's Modulus (MPa)	Damping Ratio	Poisson's Ratio
Aluminum	2.69	71,000	5×10^{-3}	0.33
Aluminum Bronze	7.89	105,000	5×10^{-2}	0.31

The modal analysis of the structure was simulated using the impact hammer test, and the location of the impact load is illustrated in Figure 14. Fifty-six points marked by red points were considered for the simulation results at measurement points. The 56 points are considered to show the place of measurement of acceleration. The sum of FRFs for all points is calculated for comparing the responses. As shown in Figure 14, one face of the model is fixed, and the other side is free for the simulation of the impact hammer test. We used fixed boundary conditions to replicate the conditions that the specimen experience during operations. The z-direction (dB) velocities of two PEEK base materials with 0% and 50% fiberglass volume fractions and different coating thicknesses were analyzed and compared, as shown in Figure 15. In an acoustic analysis for NVH, the velocity response is usually applied to the surface of the structure. Figure 15 compares the velocity in the z-direction for PEEK (0% and 50% fiberglass). As shown in Figure 15, The PEEK base part with a 2 mm aluminum coating can shift the frequencies to the right because of the added coating stiffness. Additionally, the magnitude of velocity is decreased with the increase in aluminum coating thickness. Aluminum has a higher stiffness and density compared to PEEK, which can increase the overall stiffness and mass of the coated material. This can lead to a shift in the natural frequencies of the system towards higher values. Additionally, the damping properties of the aluminum coating can also affect the vibration behavior of the PEEK. A higher damping ratio can reduce the amplitude of the vibration response at a given frequency, which can be detected in the velocity response analysis as a change in the peak amplitude or shape of the frequency spectrum. Furthermore, the 0% fiberglass shows higher damping. The peaks in Figure 15 show the resonance when the system vibrates at its natural frequency, and the velocity response peaks at this frequency. If the resonant frequency changes due to a change in the system's physical properties or boundary conditions, the velocity response peak will shift to a different frequency.

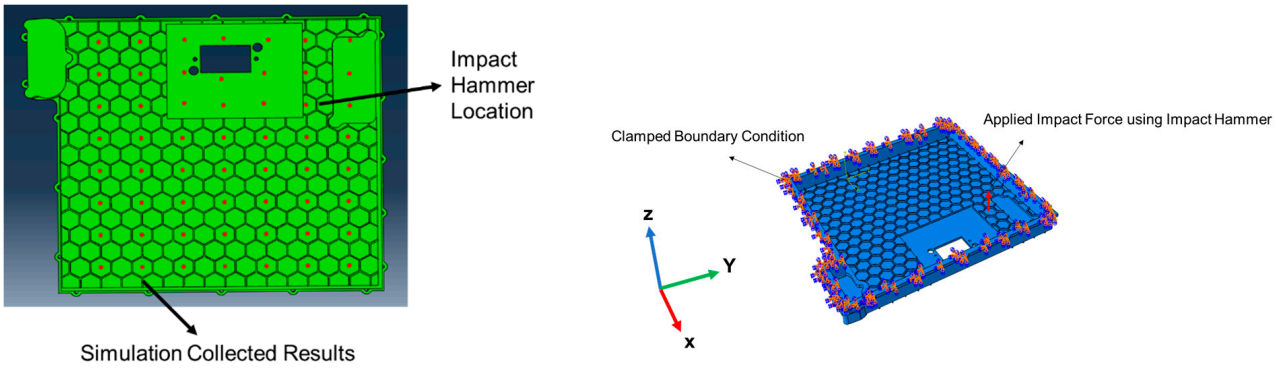

Figure 14. FE model and boundary conditions in Abaqus.

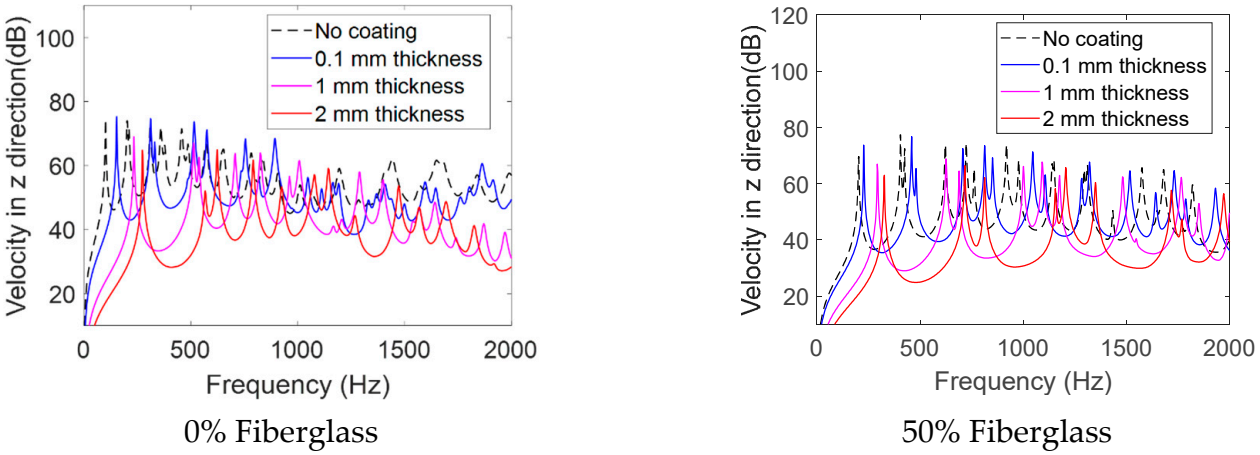

Figure 15. The sum of frequency response functions showing the velocity in the z-direction versus frequency for different PEEK and aluminum coating thicknesses obtained using a simulation.

Comparing the result of Figure 15 with previous research [54] can provide a valuable point of reference. If the results are consistent with those from previous studies, it can be concluded that the analysis is accurate.

In addition, the velocity in the z-direction (dB) (see Figure 14 for the coordinates of the model) was analyzed and compared for different aluminum bronze coating thicknesses, namely 0.1 mm, 1 mm, and 2 mm, and two PEEK base materials with 0% and 50% fiberglass, as shown in Figure 16. As can be seen in Figure 16, The PEEK base part with a 2 mm aluminum bronze coating can shift the frequencies to the right. Additionally, it can be observed that the higher aluminum bronze coating significantly reduces the velocity in higher frequencies. Adding an aluminum bronze coating to PEEK can also shift the velocity of the surface of the material. The addition of an aluminum bronze coating to PEEK can alter the natural frequencies and modes of vibration of the composite material. Similar to aluminum, aluminum bronze is a relatively stiff material compared to PEEK. The stiffness of the coating can increase the overall stiffness of the composite material, which can lead to a shift in the natural frequencies of the system towards higher values. Additionally, the damping properties of the aluminum bronze coating can also affect the vibration behavior of the PEEK.

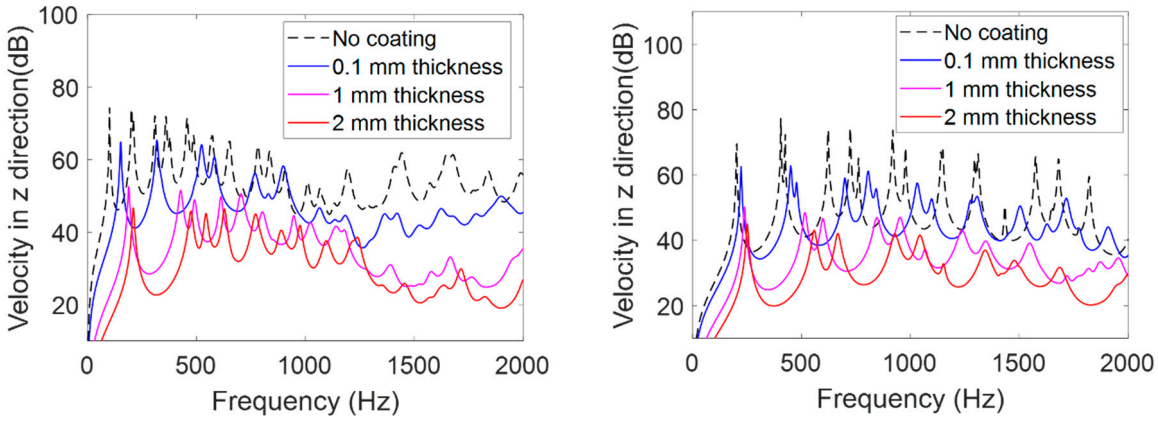

Figure 16. The sum of frequency response functions showing the velocity in the z-direction versus the frequency for a different PEEK with aluminum bronze coating was obtained using an FE simulation.

The aluminum coating can shift the frequency more than the aluminum bronze coating when comparing aluminum and aluminum bronze coatings. This occurs because aluminum has a higher stiffness-to-mass ratio. On the other hand, the higher damping ratio for aluminum bronze can effectively dampen the response, especially at higher frequencies.

4. Conclusions

In this study, we applied EMA and FEA to a sample polymer with different fiberglass volume fractions and analyzed the microstructure model in Abaqus. The work provided a framework for improving the damping properties of structures using a multi-scale simulation. The effects of different fiberglass volume ratios and their directions were studied using an FEM. Additionally, the effect of coating and microstructure in modal analysis were analyzed using FE models. The numerical and experimental modal analysis indicated that the fiberglass volume ratios and their direction could affect the damping coefficient of the structure and its vibrational properties. In other words, a high fiberglass volume increases the natural frequency of PEEK samples. In this study, the fiberglass volume ratio and direction change could change the damping ratio. Modal analysis results show that the resonance frequency was shifted to the right by increasing the thickness of the aluminum and aluminum bronze coatings. The 2 mm aluminum and aluminum bronze coatings could perform better than low-thickness coatings. The aluminum coating could shift the frequency more than the aluminum bronze coating. Additionally, it was seen that coating with a higher damping ratio (i.e., aluminum bronze) could significantly decrease the amplitude of surface velocity due to excitation, especially at higher frequencies. This is critical for electric vehicles because, in many cases, the noise occurs at higher frequency ranges.

Author Contributions: Methodology, Software, Computer Code and Supporting Algorithms, Formal analysis, Validation, Investigation, Data Curation, Writing—Original Draft, Visualization, S.J.M.Y.; Writing—Review and Editing, Resources, Formal analysis, S.P.; Investigation, Formal analysis, F.R.; Conceptualization, Software, Writing—Review and Editing, Formal analysis, Visualization, Supervision, Project administration, Funding acquisition, J.B. All authors have read and agreed to the published version of the manuscript.

Funding: The research presented in this paper is partially supported by General Motors and NSF awards #1725938 and #1625987. Any opinions, findings, conclusions, and recommendations expressed in this material are those of the author(s) and do not necessarily reflect the views of the sponsoring organizations.

Data Availability Statement: The data presented in this study are available on request from the corresponding author. The data are not publicly available because each request for sharing the data needs to be approved by the sponsor.

Conflicts of Interest: The authors declare no conflict of interest.

References

1. Zhou, W.; Cleaver, C.J.; Dunant, C.F.; Allwood, J.M.; Lin, J. Cost, range anxiety and future electricity supply: A review of how today's technology trends may influence the future uptake of BEVs. *Renew. Sustain. Energy Rev.* **2023**, *173*, 113074. [CrossRef]
2. Chakraborty, P.; Parker, R.; Hoque, T.; Cruz, J.; Du, L.; Wang, S.; Bhunia, S. Addressing the range anxiety of battery electric vehicles with charging en route. *Sci. Rep.* **2022**, *12*, 5588. [CrossRef] [PubMed]
3. Kim, K.; Choi, I. *Design Optimization Analysis of Body Attachment for NVH Performance Improvements*; SAE Technical Paper 2003-01-1604; SAE International: Warrendale, PA, USA, 2003.
4. Krishnasarma, A.; Mostafavi Yazdi, S.J.; Taylor, A.; Ludwigsen, D.; Baqersad, J. Acoustic Signature Analysis and Sound Source Localization for a Three-Phase AC Induction Motor. *Energies* **2021**, *14*, 7182. [CrossRef]
5. Kim, J.-S.; Jeong, U.-C.; Seo, J.-H.; Kim, Y.-D.; Lee, O.-D.; Oh, J.-E. Structure borne noise control of a clamped panel using shunt damping system. *Sens. Actuators A Phys.* **2015**, *233*, 330–348. [CrossRef]
6. Krishnasarma, A.; Taylor, A.; Baqersad, J.; Poozesh, P. *Structural Vibration and Acoustic Analysis of a 3-Phase AC Induction Motor*; SAE Technical Paper 2019-01-1458; SAE International: Warrendale, PA, USA, 2019.
7. Mostafavi Yazdi, S.J.; Lisitski, A.; Pack, S.; Hiziroglu, H.R.; Baqersad, J. Analysis of Shielding Effectiveness against Electromagnetic Interference (EMI) for Metal-Coated Polymeric Materials. *Polymers* **2023**, *15*, 1911. [CrossRef] [PubMed]
8. Itu, C.; Vlase, S.; Marin, M. A Vibration Analysis of the Rubber Inertial Dampers Used in Electrical Vehicles. *Polymers* **2022**, *14*, 953. [CrossRef]
9. Dziechciarz, A.; Popp, A.; Marțiș, C.; Sułowicz, M. Analysis of NVH Behavior of Synchronous Reluctance Machine for EV Applications. *Energies* **2022**, *15*, 2785. [CrossRef]
10. Garafolo, N.G.; Farhad, S.; Koricherla, M.V.; Wen, S.; Esmaeeli, R. Modal Analysis of a Lithium-Ion Battery for Electric Vehicles. *Energies* **2022**, *15*, 4841. [CrossRef]
11. Yang, F.; Sedaghati, R.; Esmailzadeh, E. Vibration suppression of structures using tuned mass damper technology: A state-of-the-art review. *J. Vib. Control* **2021**, *28*, 812–836. [CrossRef]
12. Bae, S.-Y.; Bae, K.-M.; Kim, Y.-H. Evaluation of Mechanical and Vibration Characteristics of Laminated Damping Aluminum Panel for Automobile Components. *Compos. Res.* **2019**, *32*, 113–119.
13. Kim, I.; Song, M.; Kim, J. Effects of Ti–B and Si additions on microstructure and mechanical properties of Al–Cu–Mg based aluminum matrix composites. *J. Alloys Compd.* **2020**, *832*, 154827. [CrossRef]
14. Prasad, M.; Thanikaikarasan, S. Experimental investigation and material characterization of rubber engine mount for automobile application. *Mater. Today Proc.* **2020**, *33*, 4139–4141. [CrossRef]
15. Gudetti, J.P.; Yazdi, S.J.M.; Baqersad, J.; Peters, D.; Ghamari, M. *Data-Driven Modeling of Linear and Nonlinear Dynamic Systems for Noise and Vibration Applications*; SAE Technical Paper 2023-01-1078; SAE International: Warrendale, PA, USA, 2023.
16. Kuppast, V.V. NVH Analysis of Acoustic Materials; SSRN 3924050. 2021. Available online: https://ssrn.com/abstract=3924050 (accessed on 15 September 2022).
17. Liu, X. Research on Improvement Methods of Automotive NVH Performance. In *IOP Conference Series: Materials Science and Engineering*; IOP Publishing: Bristol, UK, 2020; p. 012011.
18. Keleshteri, M.M.; Jelovica, J. Analytical assessment of nonlinear forced vibration of functionally graded porous higher order hinged beams. *Compos. Struct.* **2022**, *298*, 115994. [CrossRef]
19. Keleshteri, M.M.; Jelovica, J. Nonlinear vibration behavior of functionally graded porous cylindrical panels. *Compos. Struct.* **2020**, *239*, 112028. [CrossRef]
20. Keleshteri, M.M.; Jelovica, J. Nonlinear vibration analysis of bidirectional porous beams. *Eng. Comput.* **2022**, *38*, 5033–5049. [CrossRef]
21. Mohammadzadeh Keleshteri, M. Nonlinear Vibration Behavior of Metal Foam Structures. Ph.D. Thesis, University of British Columbia, Vancouver, BC, Canada, 2022.
22. Keleshteri, M.M.; Jelovica, J. Analytical solution for vibration and buckling of cylindrical sandwich panels with improved FG metal foam core. *Eng. Struct.* **2022**, *266*, 114580. [CrossRef]
23. Keleshteri, M.M.; Jelovica, J. Beam theory reformulation to implement various boundary conditions for generalized differential quadrature method. *Eng. Struct.* **2022**, *252*, 113666. [CrossRef]
24. Liao, L.; Zuo, Y.; Meng, H.; Liao, X. Research on the technology of noise reduction in hybrid electric vehicle with composite materials. *Adv. Mech. Eng.* **2018**, *10*, 1687814018766916. [CrossRef]
25. Han, Y.; Kumon, R.; Mostafavi Yazdi, S.J.; Zhu, N.; Afshar, A.; Baqersad, J. Nondestructive evaluation of carbon-fiber composites using digital image correlation, acoustic emission, and optical based modal analysis. *Wind Eng.* **2022**, *46*, 1618–1628. [CrossRef]

26. Xu, X.; Tang, C.; Wang, H.; An, Y.; Zhao, Y. Microstructure evolution and grain refinement mechanism of rapidly solidified single-phase copper based alloys. *J. Mater. Sci. Technol.* **2022**, *128*, 160–179. [CrossRef]
27. Hao, M.; Li, P.; Li, X.; Zhang, T.; Wang, D.; Sun, Q.; Liu, L.; Li, J.; Cui, Y.; Yang, R.; et al. Heterogeneous precipitate microstructure in titanium alloys for simultaneous improvement of strength and ductility. *J. Mater. Sci. Technol.* **2022**, *124*, 150–163. [CrossRef]
28. Xu, S.; Zhu, C.; Lin, Z.; Jin, C.; Kamado, S.; Oh-ishi, K.; Qin, Y. Dynamic microstructure evolution and mechanical properties of dilute Mg-Al-Ca-Mn alloy during hot rolling. *J. Mater. Sci. Technol.* **2022**, *129*, 1–14. [CrossRef]
29. Baqersad, J.; Poozesh, P.; Niezrecki, C.; Avitabile, P. Photogrammetry and optical methods in structural dynamics—A review. *Mech. Syst. Signal Process.* **2018**, *86*, 17–34. [CrossRef]
30. Khadka, A.; Afshar, A.; Zadeh, M.; Baqersad, J. Strain monitoring of wind turbines using a semi-autonomous drone. *Wind Eng.* **2021**, *46*, 296–307. [CrossRef]
31. Mange, A.; Atkinson, T.; Bastiaan, J.; Baqersad, J. An Optical-Based Technique to Obtain Vibration Characteristics of Rotating Tires. *SAE Int. J. Veh. Dyn. Stab. NVH* **2019**, *3*, 197–208. [CrossRef]
32. Panchal, R.; Horton, L.; Poozesh, P.; Baqersad, J.; Nasiriavanaki, M. Vibration analysis of healthy skin: Toward a noninvasive skin diagnosis methodology. *J. Biomed. Opt.* **2019**, *24*, 015001. [CrossRef]
33. Burdess, J.S.; Harris, A.J.; Wood, D.; Pitcher, R.J.; Glennie, D. A system for the dynamic characterization of microstructures. *J. Microelectromech. Syst.* **1997**, *6*, 322–328. [CrossRef]
34. Xiong, L.; Zhou, Q.; Wu, Y.; Chen, P. New laser excitation method for modal analysis of microstructure. *Mech. Syst. Signal Process.* **2015**, *50*, 227–234. [CrossRef]
35. Zhou, N.; Zhong, S.; Lin, J.; Luo, M.; Nsengiyumva, W.; Peng, Z.; Yu, Y. Acoustic-excitation optical coherence vibrometer for real-time microstructure vibration measurement and modal analysis. *IEEE Trans. Instrum. Meas.* **2020**, *69*, 7209–7217. [CrossRef]
36. Madej, L. Digital/virtual microstructures in application to metals engineering—A review. *Arch. Civ. Mech. Eng.* **2017**, *17*, 839–854. [CrossRef]
37. Bostanabad, R.; Zhang, Y.; Li, X.; Kearney, T.; Brinson, L.C.; Apley, D.W.; Liu, W.K.; Chen, W. Computational microstructure characterization and reconstruction: Review of the state-of-the-art techniques. *Prog. Mater. Sci.* **2018**, *95*, 1–41. [CrossRef]
38. Ahmadi, M.; Ansari, R.; Hassanzadeh-Aghdam, M. Micromechanical analysis of elastic modulus of carbon nanotube-aluminum nanocomposites with random microstructures. *J. Alloys Compd.* **2019**, *779*, 433–439. [CrossRef]
39. Gain, A.K.; Zhang, L.; Chan, Y. Microstructure, elastic modulus and shear strength of alumina (Al2O3) nanoparticles-doped tin–silver–copper (Sn–Ag–Cu) solders on copper (Cu) and gold/nickel (Au/Ni)-plated Cu substrates. *J. Mater. Sci. Mater. Electron.* **2015**, *26*, 7039–7048. [CrossRef]
40. Iturrondobeitia, M.; Ibarretxe, J.; Jimbert, P.; Fernandez-Martínez, R. Quantitative electron tomography of polylactic acid/clay nanocomposites for better comprehension of processing–microstructure–elastic modulus. *Polym. Polym. Compos.* **2021**, *29*, 724–732. [CrossRef]
41. Herriott, C.; Li, X.; Kouraytem, N.; Tari, V.; Tan, W.; Anglin, B.; Rollett, A.D.; Spear, A.D. A multi-scale, multi-physics modeling framework to predict spatial variation of properties in additive-manufactured metals. *Model. Simul. Mater. Sci. Eng.* **2019**, *27*, 025009. [CrossRef]
42. Al Jahwari, F.; Naguib, H.E. Finite element creep prediction of polymeric voided composites with 3D statistical-based equivalent microstructure reconstruction. *Compos. Part B Eng.* **2016**, *99*, 416–424. [CrossRef]
43. Bagheri, B.; Mahdian Rizi, A.A.; Abbasi, M.; Givi, M. Friction Stir Spot Vibration Welding: Improving the Microstructure and Mechanical Properties of Al5083 Joint. *Metallogr. Microstruct. Anal.* **2019**, *8*, 713–725. [CrossRef]
44. Amirian, A.; Torshizi, S.E.M.; Dibajian, S.H. Experimental and numerical investigation of the effect of microstructural changes on the vibrational characteristics of ck35 steel. *Proc. Inst. Mech. Eng. Part C J. Mech. Eng. Sci.* **2022**, *236*, 1363–1376. [CrossRef]
45. Damir, A.N.; Elkhatib, A.; Nassef, G. Prediction of fatigue life using modal analysis for grey and ductile cast iron. *Int. J. Fatigue* **2007**, *29*, 499–507. [CrossRef]
46. Koutoati, K.; Mohri, F.; Carrera, E. A finite element approach for the static and vibration analyses of functionally graded material viscoelastic sandwich beams with nonlinear material behavior. *Compos. Struct.* **2021**, *274*, 114315. [CrossRef]
47. Wu, J.; Habibi, M. Dynamic simulation of the ultra-fast-rotating sandwich cantilever disk via finite element and semi-numerical methods. *Eng. Comput.* **2022**, *38*, 4127–4143. [CrossRef]
48. He, Y.; Xiao, Y.; Liu, Y.; Zhang, Z. An efficient finite element method for computing modal damping of laminated composites: Theory and experiment. *Compos. Struct.* **2018**, *184*, 728–741. [CrossRef]
49. Teotia, M.; Soni, R. Applications of finite element modelling in failure analysis of laminated glass composites: A review. *Eng. Fail. Anal.* **2018**, *94*, 412–437. [CrossRef]
50. Groeber, M.A.; Jackson, M.A. DREAM.3D: A Digital Representation Environment for the Analysis of Microstructure in 3D. *Integr. Mater. Manuf. Innov.* **2014**, *3*, 56–72. [CrossRef]
51. *D638M-10*; Standard Test Method for Tensile Properties of Plastics (Metric). ASTM: West Conshohocken, PA, USA, 1992; Volume 10, pp. 172–180.

52. Friedrich, K.; Almajid, A.A. Manufacturing aspects of advanced polymer composites for automotive applications. *Appl. Compos. Mater.* **2013**, *20*, 107–128. [CrossRef]
53. Smith, M. *ABAQUS/Standard User's Manual*; Version 6.9; Simulia: Johnston, RI, USA, 2009.
54. Yılmaz, İ.; Arslan, E.; Çavdar, K. Experimental and numerical investigation of sound radiation from thin metal plates with different thickness values of free layer damping layers. *Acoust. Aust.* **2021**, *49*, 459–472. [CrossRef]